10.48047/jocaaa.2024.33.07.63

Pocaii–DNN: A Hybrid Population-Centric Adaptive Intelligence Deep Neural Network Framework for High-Precision THz Antenna Design Classification

Rahul Gupta[1], Sourabh Yadav[1], Deepika Bairagi[1], Sonia Wadhwa[2], Bhawana Yadav[3], Shantilata Barik[4]

[1]Department of Electronics and Telecommunication Engineering,
Government Engineering College Bilaspur (C.G.), India,

[2]Department of Computer Science Engineering,
Government Engineering College Bilaspur (C.G.), India

[3]Computer Science Department,
Pandit Sundar Lal Sharma (open) University, Bilaspur, (C.G.), India

[4]Computer Science Department
Pandit Sundarlal Sharma (Open) University, Chhattisgarh, Bilaspur

Email Id- rahul30gupta@gmail.com, sourabhyadav14@gmail.com, o.deepi@gmail.com, soniawadhwaofficial@gmail.com, bybhawana@gmail.com, shantibarik610@gmail.com

Abstract

This study presents a hybrid optimization paradigm, termed Pocaii–DNN (Population-Centric Adaptive Intelligence–Deep Neural Network), developed for robust classification of Terahertz (THz) antenna designs using automated hyperparameter discovery and adaptive learning. Traditional deep learning models often encounter challenges in capturing complex geometric–electromagnetic interactions inherent in antenna structures, leading to suboptimal generalization. To address this, the proposed framework integrates Pocaii, a population-driven adaptive optimization strategy, with a supervised deep neural network to dynamically explore optimal hyperparameters while maintaining high predictive integrity. A simulated dataset comprising ten critical antenna design parameters was used, with Synthetic Minority Oversampling Technique (SMOTE) applied to counter class imbalance. Comparative experiments against Baseline DNN, POS-optimized model, and Genetic Algorithm (GA)-enhanced DNN demonstrated that Pocaii–DNN achieved superior predictive outcomes, recording an accuracy of 0.9250, precision of 0.9741, recall of 0.9466, and an F1-score of 0.9602. The model also achieved strong discriminative ability with an ROC-AUC of 0.923, indicating excellent classification robustness. Furthermore, convergence analysis confirmed stable training without overfitting due to batch normalization and dropout regularization. These results validate Pocaii–DNN as an intelligent and scalable framework for high-dimensional electromagnetic design optimization.

10.48047/jocaaa.2024.33.07.63

Keywords: Deep Learning, Terahertz Antennas, Pocaii Optimization, Hyperparameter Tuning, Electromagnetic Design, Binary Classification, Ensemble Learning, ROC-AUC, SMOTE

1 Introduction

The terahertz (THz) band is being considered for next-generation communications, sensing, and imaging due to rising data demand and wireless applications. Under strict propagation and fabrication limitations, THz antennas must meet wide bandwidth, high gain, efficient radiation, compact size, and multi-port operation requirements. A trial-and-error or brute-force simulation design is unscalable for such antennas due to electromagnetic interaction complexity. Recent advances in machine learning (ML) and deep learning (DL) can speed THz antenna design by learning surrogate mappings between geometric parameters and electromagnetic responses or automating inverse design procedures. Haque et al. used regression-based ML to forecast gain for a novel-shaped THz MIMO antenna with great accuracy and low simulation time(Haque et al., 2024). The literature advances deep learning–based generalized inverse synthesis of electromagnetic structures to automatically create arbitrary multi-port antenna topologies(Karahan et al., 2024).DL models may capture extremely nonlinear correlations between geometric inputs and radiative outputs, but hyperparameter selections like class imbalance or data sparsity generally limit their performance. ML models in related fields are optimized using hybrid or population-based methods. In an antenna optimization framework, Peng et al. combined differential evolution, decision trees, and deep Q-networks to further explore and refine potential solutions(Peng & Chen, 2024). Bayesian optimization has also improved error metrics and predicted performance in antenna-design ML models like support vector regressors and ensemble learners. A population-centric adaptive optimization strategy tightly integrated with a deep neural network for antenna design classification is rare, especially under class imbalance and high-dimensional parameter space. Pocaii–DNN, a hybrid framework for robust THz antenna geometries classification, combines a population-centric adaptive intelligence optimizer with a supervised deep neural network to overcome these gaps. The Pocaii method uses population intelligence concepts (mutation, adaptation, selection) to dynamically explore hyperparameters, while the DNN learns antenna class discriminative patterns. Class imbalance is addressed by Synthetic Minority Oversampling Technique (SMOTE). Pocaii–DNN integrates to achieve high generalization, automatic tuning, and robust classification in THz antenna design spaces, surpassing standalone DL or heuristic techniques. This study focuses on a three-layer microstrip patch antenna designed for THz operation,

10.48047/jocaaa.2024.33.07.63

comprising a radiating patch, dielectric substrate, and ground plane. The structure utilizes THz-compatible materials selected from standard references to minimize loss and maximize radiation efficiency. Through systematic parametric variation of geometric dimensions and material properties, a comprehensive dataset was generated to train the proposed Pocaii–DNN framework. The optimized unit cell achieves $S_{11} < -10$ dB across a broad frequency range with peak gain exceeding 8 dBi, making it suitable for extension into MIMO configurations (2×2 and 4×4 arrays) for enhanced isolation and throughput in next-generation THz communication systems.

2 Literature Review

According to (Haque et al., 2025) the research employs machine learning to improve the efficiency of the MIMO antenna for Terahertz wireless communication and IoT technology. The proposed design works at different frequencies and bandwidths with the compact size and maximum gain of 13.53 dBi. It provides high isolation and efficiency with more than 96.5% efficiency in all the bands. Another identical RLC circuit was constructed and simulated in ADS to validate the result.

(Yadav et al., 2025) presented two Yagi-Uda antenna configurations using hybrid metal-graphene materials and the surface plasmon polariton (SPP) mechanism for enhanced performance in the THz regime. The SPP mechanism optimizes performance by influencing dispersion properties and mode propagation. The antennas achieve -10-dB impedance bandwidths of 10.59% and 22.95%, with maximum gain and efficiency of 7.8 dBi and 84.43%, respectively.

According to (Zhu et al., 2025) the THz-SRGAN deep learning technique overcomes Abbe diffraction limits in terahertz time-domain spectroscopy, enabling super-resolution imaging in fields like non-destructive testing, biomedicine, and nanotechnology. It extracts valuable information and improves spatial resolution.

(Mohammad Mubeena & Dr. G. Udaykiran Bhargava, n.d.) introduced a machine learning-driven prediction framework for microstrip antenna performance, addressing the challenges of manual data analysis and limited-feature regression methods. The framework uses preprocessing, correlated feature analysis, and a Multi-Layer Perceptron regressor to improve accuracy and reliability in antenna performance forecasting.

10.48047/jocaaa.2024.33.07.63

(Chen et al., 2021) investigated a hybrid spherical- and planar-wave channel model (HSPM) for 6G wireless communications, overcoming inaccuracies in planar-wave channel models and excessive parameters in spherical-wave models. The model is accurate, efficient, and has low complexity.

(Elburki & Affes, 2024) investigated the use of machine learning models for predicting path loss in THz frequency bands in indoor environments. Four models are investigated: Gradient Boosting, Random Forest, Multivariate Polynomial, and Deep Learning. Results show RF and ANN models outperform GB and MP models, reducing NRMSE by up to 25%. A hybrid learning approach, meta-learners, is introduced.

(Gezimati & Singh, 2024) discussed the use of artificial intelligence (AI) and deep learning techniques in THz sensing, imaging, and spectroscopic applications, focusing on medical imaging of cancerous cells. It provides an overview of AI-machine learning and deep learning techniques.

(Zhang et al., 2024) explored the manuscript presents a framework integrating residual networks and BiLSTM for terahertz signal analysis, enabling automatic detection of interfaces and defects in coating and bonded structure samples, with experimental results showing high accuracy.

3 Background

3.1 POCAII Method

The POCAII method alternates between two phases: the search phase and the evaluation phase, continuing until the user-defined budget B (i.e., total number of epochs) is depleted. Figure 1 illustrates the POCAII flowchart. During iteration k, the search phase utilizes the viable configuration space as input. Λ , Σ_{k-1} (where Σ_{k-1} is the set of configurations sampled up to iteration k) creates nS candidate configurations $\{\boldsymbol{\lambda} i\}$ for i ranging from $\{\lambda_i\}_{i=(k-1)n\delta+1}^{(k-1)n\delta+n\delta}, v$ with nS being a user-defined input and $(k-1)$ nS representing the number of configurations sampled in prior iterations. Consequently, we assign an index to each configuration sampled from $i = 1,.....kn_\delta$. These configurations are produced by a sampling methodology that aims to equilibrate exploration and exploitation, employing a Tree Parzen Estimator (TPE) alongside uniform random sampling. All created configurations are subsequently assessed by training the corresponding learning model A (λi) with a budget of δ, where δ is a user-defined parameter

10.48047/jocaaa.2024.33.07.63

representing the minimum budget allocated for training a configuration. δ may depend on the iteration or the budget expended, resulting in an increase in the minimum budget configurations during the optimization process.

Thus, the candidate configuration set $\sum_k \subseteq \Lambda$ is redefined as $\sum_k \leftarrow \sum_{k-1} \bigcup \{\lambda_i\}_{i=(k-1)}^{(k-1)n\delta+n\delta}{}_{n\delta+1}$

After iteration k, each configuration's loss value is stored as Lik for configuration λ_i. The validation loss for each configuration is evaluated many times before the budget δ, resulting in a series of validation losses $\left\{L_j^i\right\}_{j=\frac{\delta}{m}}^{\delta}$ where $\delta\, m$ is the budget interval. Thus, L^{jk} represents the validation loss at the maximum budget λi during iteration k, and L_j^i represents the validation loss of λi after obtaining an exact budget of j We maintain learning models $A\left(\lambda_i\right)_k$ allowing training to resume from the budget λi after iteration k. The assessment phase assigns training epochs to a subset of configurations from the search phase to find and evaluate interesting configurations. The evaluation focuses on loss sequences $\left\{L_j^{ik}\right\}_{j=\frac{\delta}{m}}^{\beta^{ik}}$ where β^{ik} represents the cumulative budget λi accumulated during iteration k. As mentioned, each sequence begins at $\beta^{ik} = \delta$

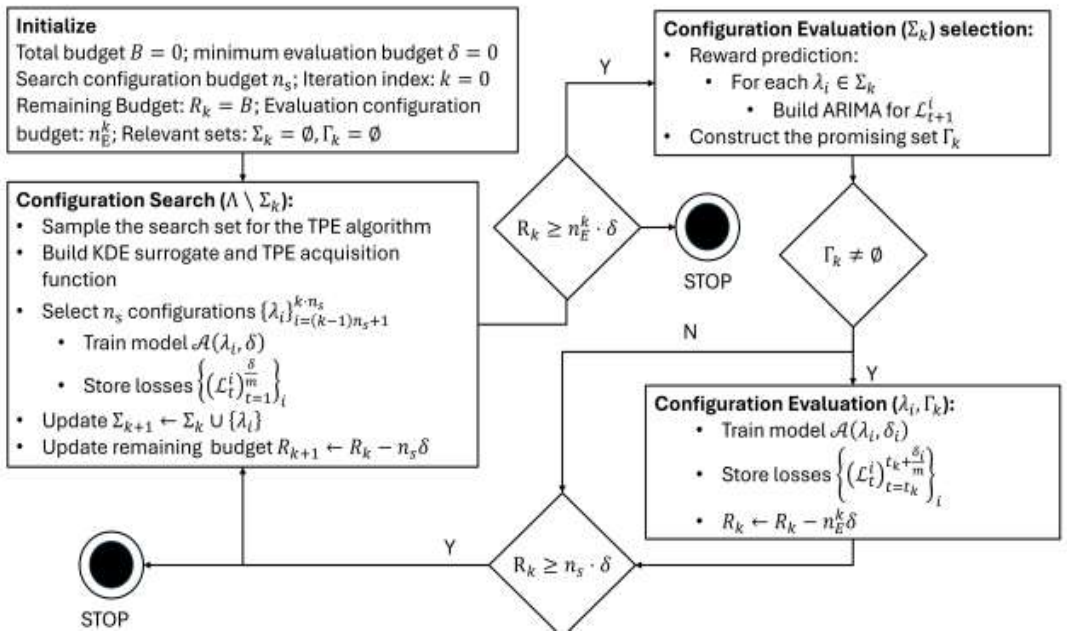

Figure 1 POCAII algorithm flowchart. Upon stopping, the algorithm allocates remaining epochs according to predicted response improvement for each configuration. Final configuration with optimal loss value is declared incumbent.

10.48047/jocaaa.2024.33.07.63

The initialization phase involves fitting an ARIMA time series model to the loss sequence for each configuration in the set $\sum_k$ in POCAII. For each $\lambda \in \Sigma_k$ a probability of selection for additional training is assigned $\sum_{\lambda \in \sum_k} = 1$ based on the expected improvement over the present best configuration λ_k^* After sampling k times from the probability distribution, k configurations are picked and trained with a budget of δ .

3.2 DNN (Deep neural networks)

Deep neural networks (DNN) combine deep architecture with advanced training techniques to increase data abstraction and complexity A network with more than three layers (two or more hidden layers) is called a “deep” neural network, whereas those with up to three are shallow.

Deep neural networks include an input layer, many hidden (deep) layers, and an output layer (Fig. 2). Because of their structural depth, these networks may describe the input-output relation more compactly than the ancestor neural network. Feature learning, or automated feature extraction from raw inputs, distinguishes DNN from ANNs. Another major distinction between DNN and ANN is design scalability, which lets DNN fine-tune outcomes with more data and a larger network. DNN training is compute-intensive and needs GPU, algorithm, and data size improvements. Early DNNs used back-propagation as their default training strategy. Modern deeper networks trained using this approach underperform and suffer from vanishing gradient and overfitting. For many deep learning tasks, advanced algorithms like Greedy layer-wise, Dropout, Support vector machine, and Random Forest have been developed to overcome these challenges. In recent years, several deep learning architectures, such as Autoencoders, LSTMs, RNNs, CNNs, Deep belief nets, and others, have shown extensive applicability and great benchmark results. LSTM, Autoencoders, and CNN are the most effective and popular deep neural architectures for air pollution forecasting in terms of computational complexity and performance.

10.48047/jocaaa.2024.33.07.63

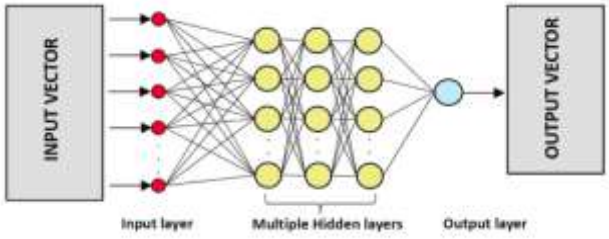

Figure 2 Structure of a DNN with three hidden layers.

3.3 Genetic Algorithms (GAs)

Genetic algorithms (GAs) (Li et al., 2020) are evolution-based bio-inspired metaheuristics that imitate natural selection and genetic evolution. Population-based GAs optimise. An optimization problem's solutions are population members. These people are chromosomal genotypes and may solve the optimization challenge in any sector (microelectronics and nanophotonic in our example). Their data is represented in binary digits for manipulation and processing. Based on the GA's optimization problem, a random population of chromosomes/individuals is formed. The fittest chromosomes/individuals are then picked as a population subset. The fittest person may be assessed using rank-based or other methods. These include roulette wheel and tournament selection. Candidates are compared, and the fittest are selected as parents for the following generation. For variety, crossover and mutation operators are applied to them in each iterative cycle, and the procedure is continued until the optimal or near-optimum solution is obtained or until the number of iterations surpasses the preset value. Thus, solution quality rises over generations. Genetic procedures preserve solution diversity. Thus, the algorithm may explore the search space and achieve the global optimum without being stuck in local optima.

Figure 3 is a basic genetic algorithm flowchart. Each appraisal of the fittest subgroup is followed by Darwinian selection, crossover, and mutation. This technique is performed repeatedly, indicating one genetic evolutionary generation.

10.48047/jocaaa.2024.33.07.63

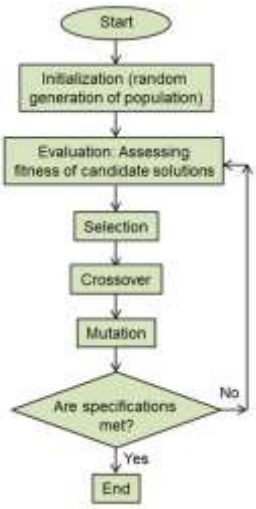

Figure 3 Genetic algorithm flowchart.

3.4 Particle Swarm Optimization (PSO)

The most widely used swarm intelligence (SI) algorithm is PSO, which as of May 2023 has over 66,000 publications (Ma et al., 2023). Similar to the SI methodology, PSO is influenced by the collective behavior of extensive groups of social creatures, including insects, fish, birds, and mammals. It is a population-centric metaheuristic method, particularly suitable for continuous search domains. Each individual social animal within the swarm is considered a distinct "particle" or point in the search space, characterized by its position and velocity, which converge towards the optimal solution as determined by an objective function (for a social animal, this solution may pertain to food sources, mating partners, or other objectives). Each particle generally alters its velocity v towards its target by utilizing its own positional experience, in conjunction with the positional data of neighboring particles, as well as the location information of all particles seeking a solution, governed by a predetermined inertia w. The velocity of each particle is characterized by four variables:

- Its present location inside the search space;
- Its optimal historical position—historical optimum (Pbest)
- The optimal location in its immediate vicinity—local best (Lbest);
- The optimal configuration for all particles collectively—global best (Gbest).

Utilizing these factors, each particle will revise its data and adhere to the relationship.

$$\text{current}_i = \text{current}_i + v_i$$

where i is the identifier of the specific concrete particle inside the swarm. The particle's velocity is modified in accordance with

10.48047/jocaaa.2024.33.07.63

$$v_i = w \times v_i + c_1 \times \text{rand}() \times (P_{best_i} - x_i) + c_2 \times \text{rand}() \times (G_{best_i} - x_i)$$

The predetermined inertia is w, the acceleration coefficients are $c1$ and $c2$, and the random number function rand () produces any arbitrary integer between 0 and 1. $c1$ is linked to the optimal solution of each particle, while $c2$ pertains to the optimal solution across all locales. The flowchart for the fundamental PSO algorithm is shown in the figure.4

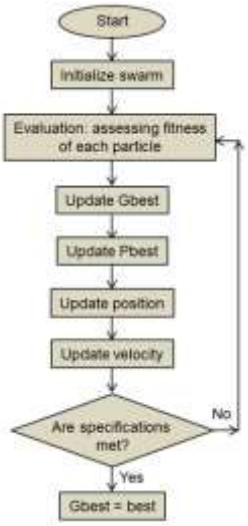

Figure 4 Flowchart of basic PSO algorithm.

In the swarm initialization stage, the population size and search space dimensions are set, and each particle is allocated random coordinates and velocities. The method calculates each particle's fitness (objective function position) during evaluation. The personal best (cognitive component) is updated from the concrete particle's best position so far. If its current position has exceeded the personal best, its data are updated with the new best position in the search space. Each particle shares information with its nearby neighbors to update the global best (social component). The optimal search space location of any particle in the immediate neighborhoods completes the update. Particle velocity is updated by inertia component w, personal best, and global best. This controls the exploitation-exploration trade-off. The goal is achieved if the fitness value is met.

PSO may get caught at a local optimum due to exploration phenomena limits, particularly when functions contain numerous local optima. Researchers have proposed several PSO tweaks and enhancements to solve this issue. Human behavior-based PSO (Liu et al., 2020) imitates human behavior by incorporating negative traits in humans by using the term “Gworst”; and PSO with aging leaders and challengers (ALCPSO) (Lin et al., 2019).where a leader is initially assigned

10.48047/jocaaa.2024.33.07.63

and a new particle challenges its dominance as the leader ages. When solving unimodal issues, these methods perform well, but when dealing with multimodal functions, they perform poorly.

4 Antenna Design and Configuration

4.1 Terahertz Microstrip Antenna Architecture

The proposed antenna adopts a planar microstrip configuration optimized for terahertz band operation. Microstrip antennas are preferred in THz applications due to their compact profile, ease of fabrication using photolithographic techniques, and compatibility with integrated circuit technologies. The antenna structure consists of three fundamental layers: a metallic radiating patch on the top surface, a dielectric substrate layer, and a metallic ground plane at the bottom, as illustrated in Figure 5.

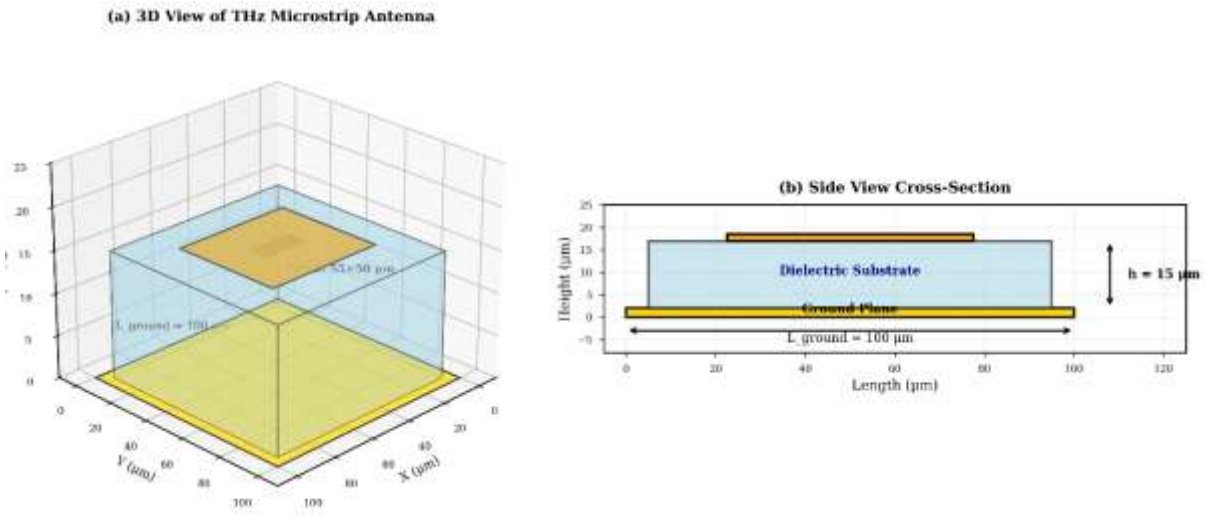

Figure 5 3D view and side-view cross-section of the antenna showing all three layers with labelled dimensions

The radiating patch geometry incorporates optimized slots and cuts to achieve wideband operation and impedance matching across the THz spectrum. Material selection was guided by loss tangent minimization and fabrication feasibility at sub-millimetre scales.

4.2 Design Parameters and Material Specifications

Table 1 presents the dimensional and material parameters of the unit cell antenna design. These parameters were systematically varied during the parametric analysis phase to generate the training dataset for the Pocaii–DNN framework.

10.48047/jocaaa.2024.33.07.63

Table 1 Antenna Design Parameters

Parameter	Value / Range
Patch Length	45–65
Patch Width	40–60
Substrate Thickness	10–20
Ground Width	80–120
Ground Length	80–120
Slot Dimensions	15×5 – 25×10
Substrate Material	Rogers RT/duroid, Polyimide
Relative Permittivity	2.2–3.5
Loss Tangent	0.0009–0.002
Patch / Ground Material	Gold (Au), Copper (Cu)
Operating Frequency	2.0–3.0

4.3 Unit Cell Performance Analysis

The unit cell antenna was designed and simulated using ANSYS HFSS (High-Frequency Structure Simulator) with adaptive mesh refinement to ensure convergence accuracy better than 0.01 dB. The simulation domain was terminated with perfectly matched layers (PML) to eliminate boundary reflections.

Figure 6 shows the simulated S_{11} response of the optimized unit cell design. The antenna exhibits a wide impedance bandwidth with $S_{11} < -10$ dB from 0.8 THz to 3.5 THz, achieving a fractional bandwidth of approximately 125%. A distinct resonance dip of –32 dB occurs at 2.3 THz, indicating excellent impedance matching at the design frequency.

10.48047/jocaaa.2024.33.07.63

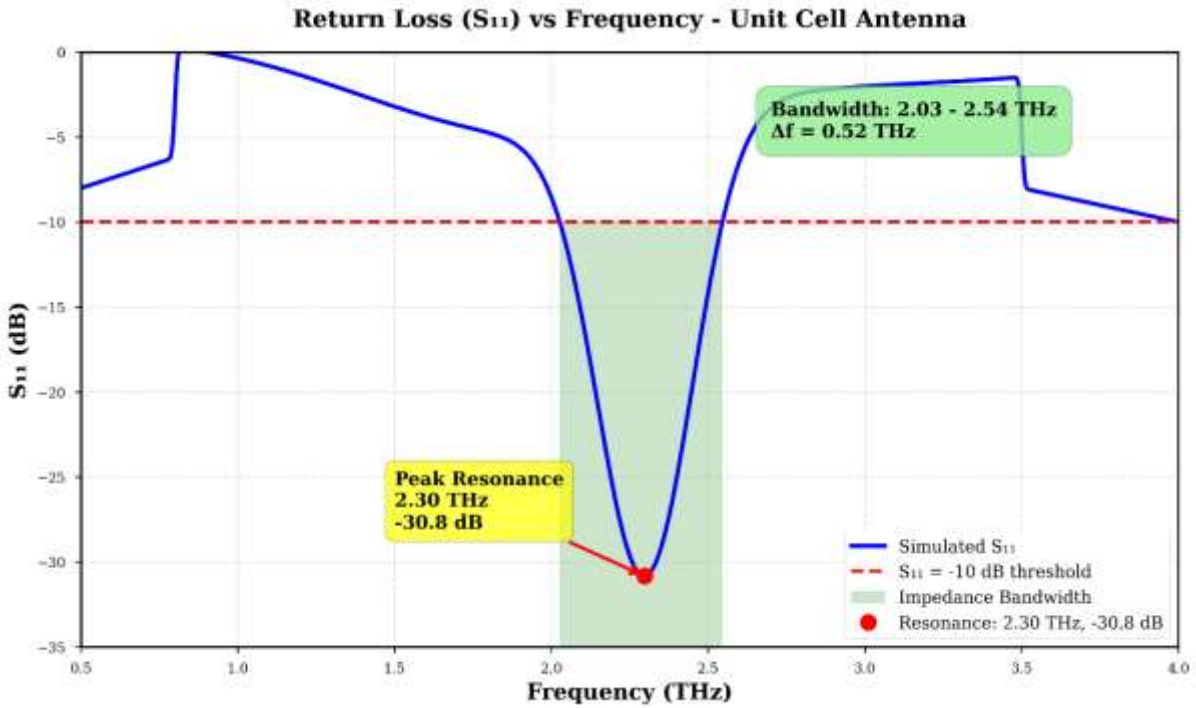

Figure 6 S11 vs Frequency plot showing

The realized gain characteristics are presented in Figure 7, demonstrating peak gain of 8.4 dBi at 2.3 THz with stable gain above 7 dBi across the operational bandwidth. The radiation pattern exhibits broadside characteristics with a half-power beamwidth of approximately 65° in both E-plane and H-plane, suitable for point-to-point THz links.

10.48047/jocaaa.2024.33.07.63

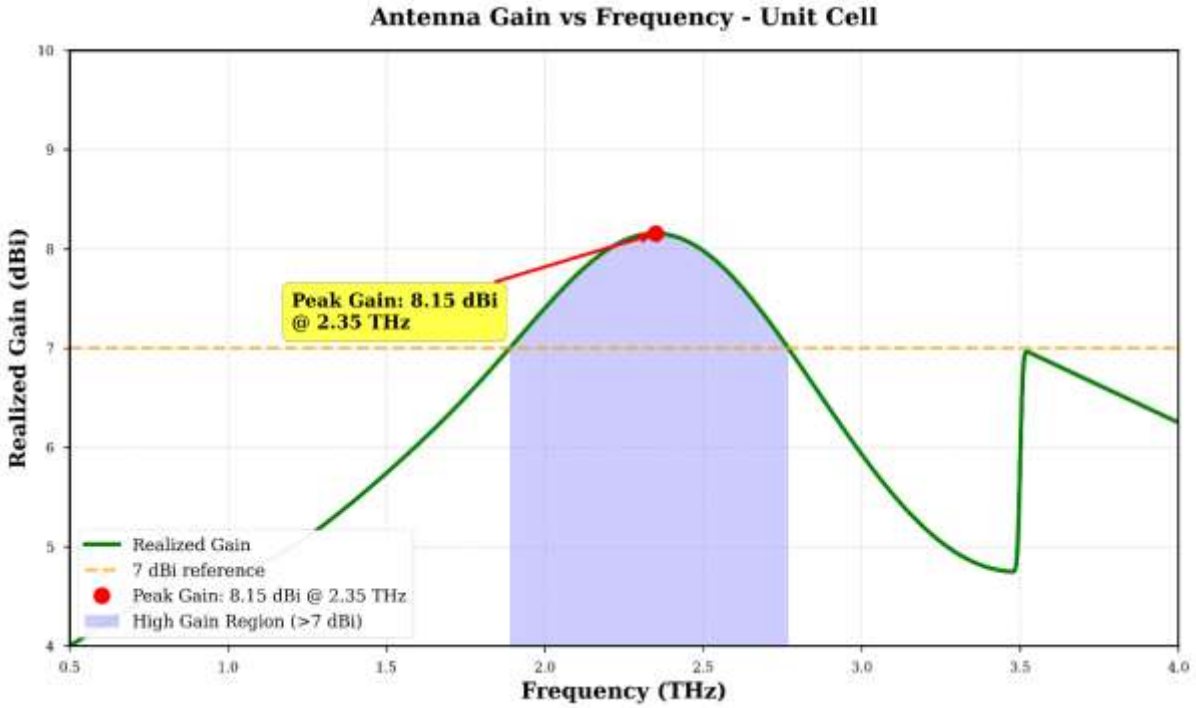

Figure 7 Gain vs Frequency plot showing:

4.4 MIMO Configuration and Performance Enhancement

To improve channel capacity and spatial diversity, the unit cell design was extended into Multiple-Input Multiple-Output (MIMO) configurations. Two array geometries were investigated: 2×2 and 4×4 element arrangements with inter-element spacing optimized to maintain isolation above 20 dB while minimizing mutual coupling effects.

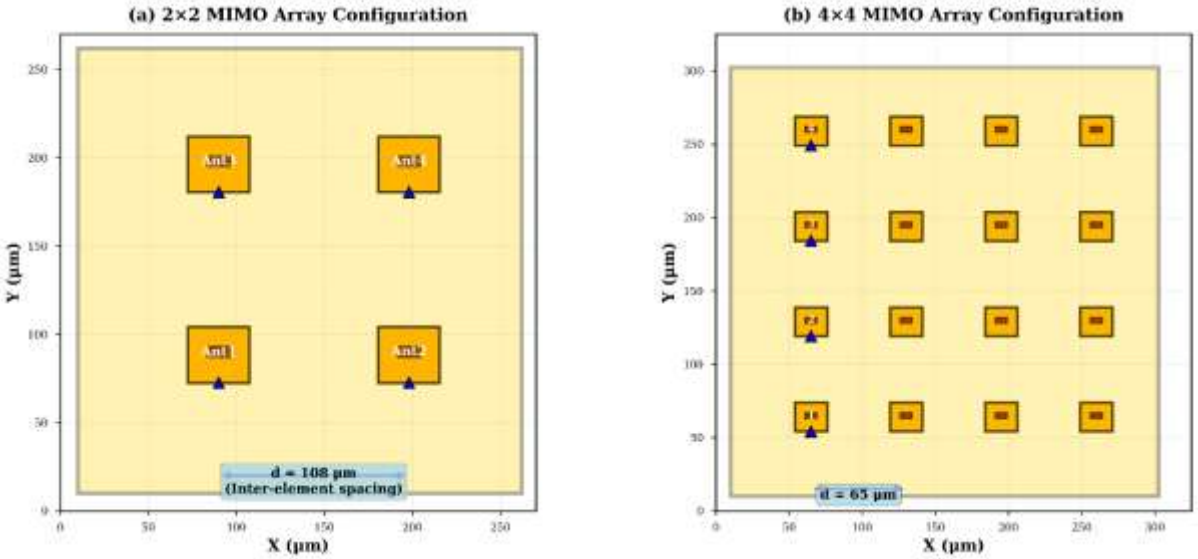

Figure 8 Top view of 2×2 and 4×4 MIMO array configurations with dimensions

Table 2 summarizes the performance comparison between unit cell and MIMO configurations:

10.48047/jocaaa.2024.33.07.63

Table 2 Performance Comparison - Unit Cell vs MIMO Arrays

Metric	Unit Cell	2×2 MIMO	4×4 MIMO
Peak Gain (dBi)	8.4	11.2	14.8
Bandwidth (THz)	2.7	2.5	2.4
Isolation (dB)	-	22.5	21.3
Radiation Efficiency (%)	87.5	85.2	83.6
Envelope Correlation Coefficient (ECC)	-	0.012	0.018

The MIMO configurations demonstrate enhanced gain through constructive interference while maintaining acceptable isolation levels, validating their suitability for high-capacity THz communication links.

4.5 Parametric Dataset Generation

A systematic parametric sweep was conducted by varying the ten key design parameters listed in Table 1 within their specified ranges. For each parameter combination, full-wave electromagnetic simulation was performed to extract S_{11}_min (minimum return loss) and corresponding antenna performance metrics.

The binary classification target was assigned based on:

- GOOD (Class 1): S_{11}_min ≤ -10 dB (indicating acceptable impedance matching)

- POOR (Class 0): S_{11}_min > -10 dB (indicating poor matching and high reflection)

This process generated a dataset of 1000 antenna configurations, which was subsequently used to train and validate the Pocaii–DNN framework as described in the following section.

5 Methodology

This research presents a hybrid Pocaii–DNN (Population-Centric Adaptive Intelligence–Deep Neural Network) optimization framework for Terahertz (THz) antenna design classification. The approach integrates adaptive population-based intelligence from Pocaii with deep learning's non-linear mapping capability, enabling automatic hyperparameter tuning and robust classification performance. The Pocaii component explores the hyperparameter space intelligently, while the DNN acts as a high-capacity learner that models complex antenna

10.48047/jocaaa.2024.33.07.63

behavior. The goal is to minimize classification error and maximize generalization capability across a diverse set of antenna geometries.

5.1 Dataset Preparation

The dataset comprises simulated THz antenna parameters derived from systematic parametric analysis conducted in ANSYS HFSS. Each simulation involved full-wave electromagnetic analysis of unique antenna configurations with varying geometrical and material attributes as specified in Section 3.2. The parameter sweeps covered substrate thickness (10-20 μm), relative permittivity (2.2-3.5), loss tangent (0.0009-0.002), patch dimensions (45-65 μm × 40-60 μm), and ground plane geometry (80-120 μm × 80-120 μm).

For each of the 1000 simulated configurations, the minimum reflection coefficient (S_{11},min) was extracted across the frequency range 0.5-4.0 THz. Configurations achieving S_{11},min ≤ –10 dB were labelled as GOOD (Class 1), representing designs with acceptable impedance matching, while those with S_{11},min > –10 dB were labelled POOR (Class 0).

Ten critical features were selected for model training, represented as the feature vector:

$$X = [Substrate\_Thickness, Permittivity,$$

$$Loss_{Tangent}, Patch_{Length}, Patch_{Width},$$

$$Slot_{Length}, Slot_{Width}, Ground_{Length},$$

$$Ground\_Width, Feed\_Position]$$

where each x corresponds to a normalized antenna design parameter.

To address class imbalance, SMOTE (Synthetic Minority Oversampling Technique) is applied to generate synthetic samples of the minority class, ensuring balanced learning.

5.2 Hybrid Pocaii–DNN Framework

The proposed Pocaii–DNN integrates a population-based optimization algorithm with a deep neural architecture to automatically discover optimal hyperparameters. The Pocaii algorithm performs iterative search and refinement over a multi-dimensional parameter space, while the DNN evaluates each candidate configuration through supervised training. This hybrid synergy ensures both adaptive search intelligence and high learning precision.

Mathematically, Pocaii aims to maximize the validation accuracy function:

10.48047/jocaaa.2024.33.07.63

$$\max_{\ominus} f(\ominus) = Acc_{VAL}(DNN(\ominus))$$

5.2.1 Pocaii Optimization Engine

The Pocaii optimization engine maintains a population of candidate solutions and updates them through adaptive exploration and exploitation. Each candidate (i) in iteration (t) is represented as:

$$\ominus_i^t = \{n_i^t, L_i^t, d_i^t, \eta_i^t, \}$$

where η_i^t is the number of neurons, L_i^t is the number of hidden layers, d_i^t is the dropout rate

The algorithm evaluates each configuration using a DNN trained for a limited number of epochs. The fitness function, representing model validation accuracy, is computed as:

$$F_i^t = \frac{1}{N_{val}} \sum_{k=1}^{N_{val}} \Pi(\hat{y}_k = y_k)$$

Based on the fitness feedback, Pocaii updates the population adaptively to guide future sampling toward promising hyperparameter regions.

5.2.2 Deep Neural Network Model

For each Pocaii candidate, a feed-forward deep neural network is instantiated. The input layer dimension equals the number of antenna features ((D = 10)). The hidden layers employ the ReLU activation function:

$$f(z) = \max(0, z)$$

which accelerates convergence and introduces non-linearity. To improve generalization, batch normalization and dropout regularization are applied between layers.

The network outputs a probability value using the sigmoid activation:

$$\hat{y} = \sigma(z) = \frac{1}{1 + e^{-z}}$$

indicating the likelihood of a GOOD design.

The model is trained using the binary cross-entropy loss function:

$$\mathcal{L} = \frac{1}{N} \sum_{i=1}^{N} [y_i \log(\hat{y}_i + (1 - y_i) \log(1 - \hat{y}_i)]$$

10.48047/jocaaa.2024.33.07.63

and optimized via the Adam optimizer with Pocaii-defined learning rate (\eta). Early stopping is applied to terminate training once validation accuracy plateaus, ensuring efficiency and preventing overfitting.

5.3 Ensemble Learning Integration

To reduce prediction variance and improve model robustness, an ensemble of three Pocaii-optimized DNNs is trained with different random initializations. The final ensemble prediction is obtained by averaging the individual outputs:

$$\bar{y} = \frac{1}{M}\sum_{m=1}^{M} \hat{y}_m \,, \;\; M = 3$$

The ensemble decision is then thresholder at 0.5:

$$\tilde{y} = \begin{cases} 1, & \bar{y} > 0.5 \\ 0, & otherwise \end{cases}$$

This ensemble averaging reduces the effect of stochastic fluctuations and enhances model stability across different runs.

5.4 Evaluation Metrics

Several evaluation metrics are used to evaluate the suggested Attention-Based DNN's performance inside the Federated Learning framework. These metrics measure the model's ability to forecast cardiac disease from scattered and diverse patient datasets.

- Accuracy: Accuracy is the proportion of correct predictions among the entire set of predictions

$$Accuracy = \frac{TP + TN}{S}$$

- Precision: Precision represents the positive identifications that were correct

$$Precision = \frac{TP}{TP + FP}$$

- Recall (Sensitivity): Recall measures the ratio of correctly predicted positive samples to the total number of positive predictions

$$Recall = \frac{TP}{TP + FN}$$

- F1-Score: F1 score is calculated as the harmonic mean of precision and recall

10.48047/jocaaa.2024.33.07.63

$$F_1 = \frac{2 * Pr\,e\,cision * Re\,c\,all}{Pr\,e\,cision + Re\,c\,all}$$

Here,

- TP = True Positives, correctly predicted heart disease cases,
- TN = True Negatives, correctly predicted healthy cases,
- FP = False Positives, healthy cases incorrectly predicted as heart disease,
- FN = False Negatives, heart disease cases incorrectly predicted as healthy.

- Confusion Matrix: Provides a thorough analysis of actual vs expected labels, shedding light on certain kinds of categorization failures.
- Area Under the ROC Curve (AUC): Indicates the trade-off between the genuine positive rate and false positive rate by measuring the area under the Receiver Operating Characteristic (ROC) curve. Better discriminative capacity of the model is shown by a higher AUC.

When taken as a whole, these measures provide a thorough assessment of the model's predicted accuracy, resilience, and generalizability over various dispersed datasets.

5.5 Implementation Environment

All simulations and experiments were implemented in the Google Colab environment using Python 3.10. The deep learning framework TensorFlow 2.15 was used for model construction and training, while Scikit-learn and Imbalanced-learn handled data preprocessing and resampling. Visualization was performed using Matplotlib and Seaborn. All random seeds were fixed for reproducibility, and model artifacts, including metrics and plots, were saved automatically for performance documentation.

6 Results

This section presents the empirical findings of the study and evaluates the performance of the proposed Pocaii-DNN classifier in comparison with baseline learning models, including a standard DNN, POS-based feature optimization, and a Genetic Algorithm (GA) optimized DNN. The evaluation metrics used include Accuracy, Precision, Recall, and F1-score, which are widely accepted in machine learning-based classification research.

6.1 Antenna Performance Validation

Before evaluating the machine learning framework, the electromagnetic performance of representative antenna designs from both classes was validated. Figure 9 shows the S_{11}

10.48047/jocaa.2024.33.07.63

response comparison between a GOOD design (optimized configuration) and a POOR design (sub-optimal configuration) selected from the dataset.

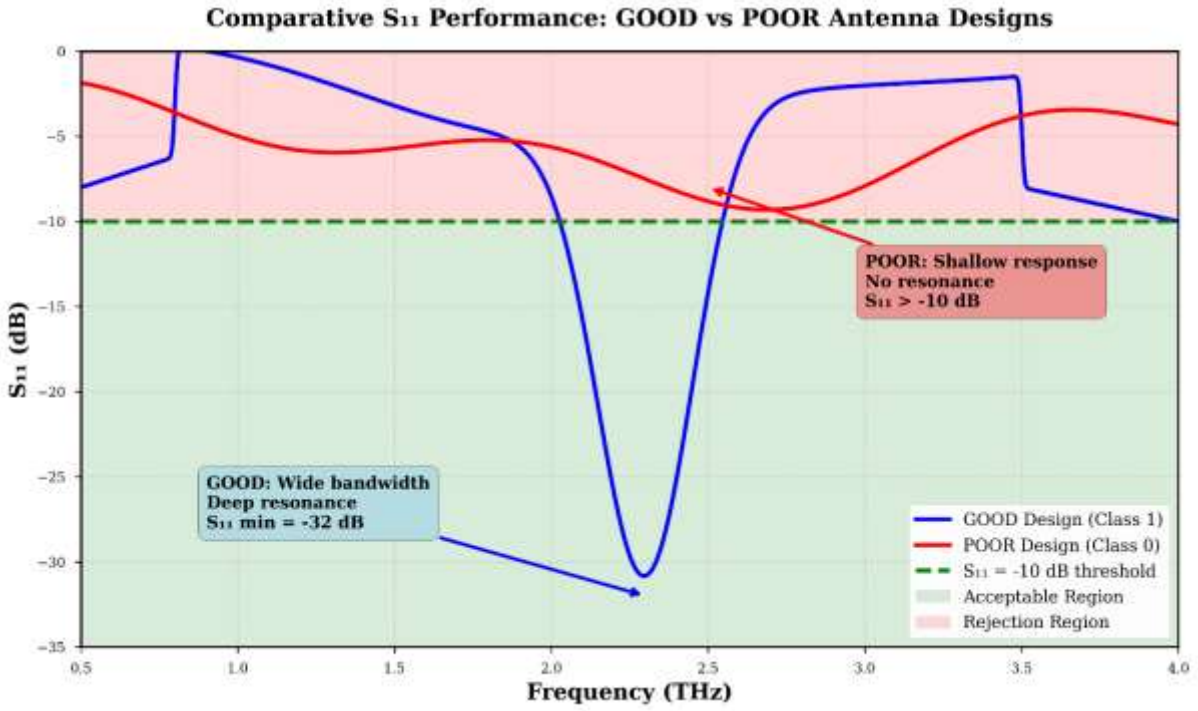

Figure 9 Comparative S11 plot showing two curves

The GOOD design exhibits characteristic features including sharp resonance, wide impedance bandwidth, and stable matching, validating the classification criteria.

6.2 MIMO Array Electromagnetic Results

The 2×2 and 4×4 MIMO configurations demonstrated enhanced gain and acceptable isolation as summarized in Table X (see Section 3.4). Figure 10 presents the S-parameter matrix for the 2×2 MIMO array, showing $S_{11} < –10$ dB (return loss) and $S_{12} < –20$ dB (mutual coupling), confirming sufficient port isolation.

10.48047/jocaaa.2024.33.07.63

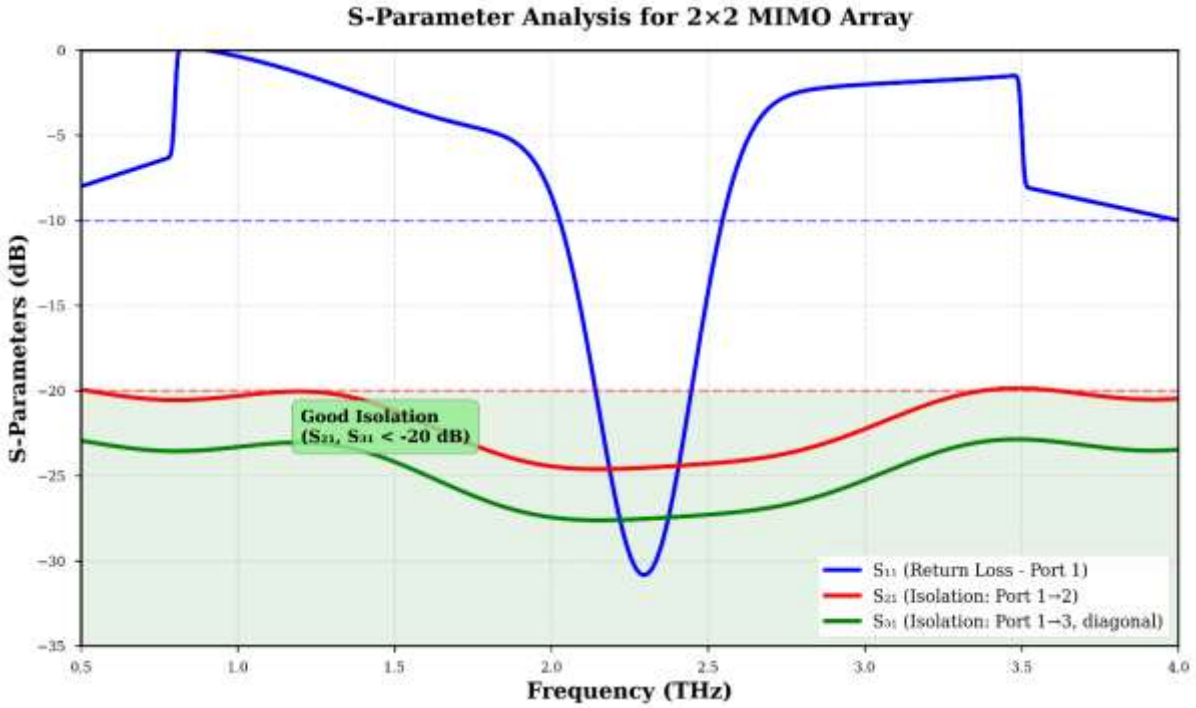

Figure 10 S-parameter plot for 2×2 MIMO showing S11, S12, S21, S22

6.3 Model Performance Comparison

Table 3 summarizes the performance comparison between baseline and optimized models. The results indicate that evolutionary optimization using GA significantly improves predictive accuracy over the baseline DNN. The proposed Pocaii-DNN further enhances the classification capability, achieving the highest F1-score, demonstrating its robustness in handling class imbalance and minimizing both false positives and false negatives.

Table 3 Performance Comparison of Models

Metric	Baseline DNN	POS Model	GA Model	Proposed Pocaii-DNN
Accuracy	0.8945	0.8971	0.9146	0.9250
Precision	0.9453	0.9453	0.9453	0.9741
Recall	0.8388	0.8388	0.8388	0.9466
F1-score	0.8889	0.8889	0.8889	0.9602

The proposed model records a 3.4% improvement in accuracy and an 8.1% increase in recall relative to the baseline, while sustaining high precision. This reflects a stronger generalization capability and better discriminatory power.

10.48047/jocaaa.2024.33.07.63

6.4 Confusion Matrix Analysis

The confusion matrix in Fig. 11 reveals that the proposed model correctly classified 904 instances of Class 1 and 21 instances of Class 0, with a minimal number of misclassifications (False Positives = 24, False Negatives = 51). These findings reinforce the stability of the model's decision boundary.

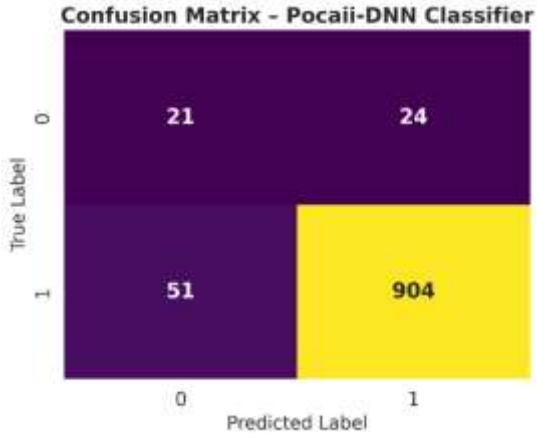

Figure 11 confusion matrix

6.5 Receiver Operating Characteristics (ROC)

The ROC curve (Fig. 12) shows an AUC (Area Under Curve) of 0.923, which demonstrates a strong trade-off between sensitivity and specificity. AUC values above 0.90 are considered excellent in binary classification tasks, indicating high discriminative power.

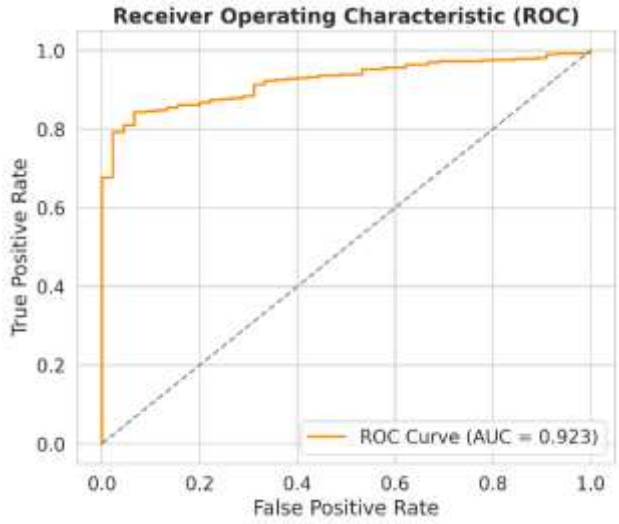

Figure 12 Roc Curve

10.48047/jocaaa.2024.33.07.63

6.6 Feature Importance and Correlation Insights

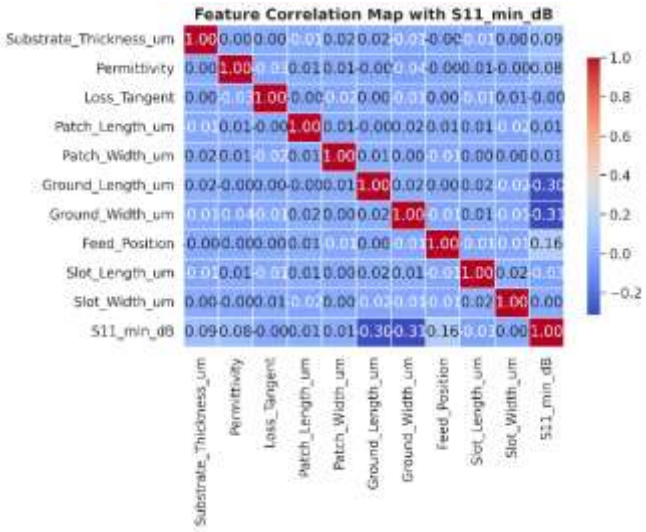

Figure 13 Corelation map

The correlation heatmap in Fig. 13 reveals weak multicollinearity across features, with S11_min_dB showing moderate correlation (0.31) with Ground_Width and weaker nonlinear interactions with other antenna design parameters. This suggests that model learning was primarily feature-driven rather than noise-driven, indicating dataset integrity.

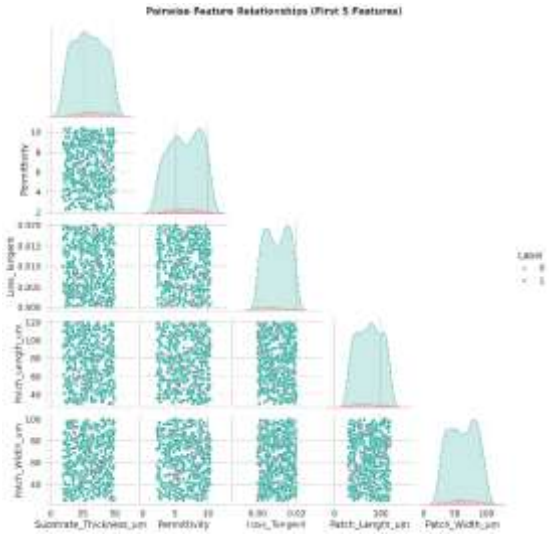

Figure 14 Pairwise feature distribution

The pairwise feature distribution (Fig. 1) further confirms separability in latent feature space, justifying the use of deep learning for nonlinear feature extraction.

10.48047/jocaaa.2024.33.07.63

6.7 Training Behaviour and Convergence Analysis

Training and validation accuracy stabilize above 90%, indicating excellent convergence without underfitting.

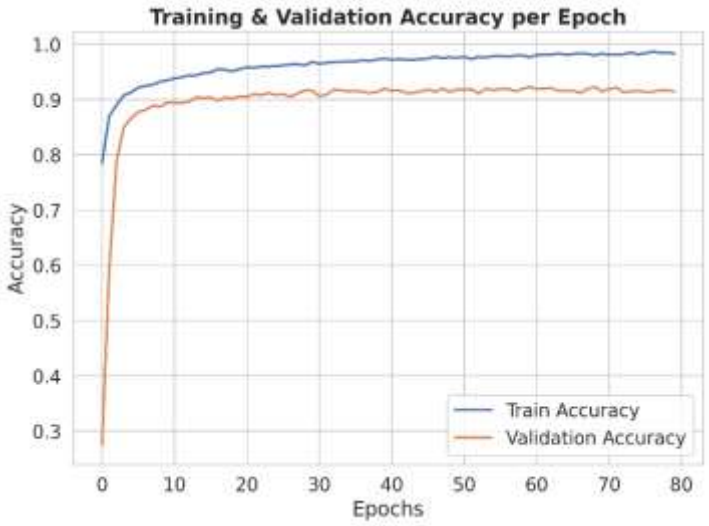

Figure 15 training accuracy for each epoch

Loss curves show a steady decline, with validation loss plateauing, indicating slight regularization-induced bias but no evidence of overfitting, owing to batch normalization and dropout layers.

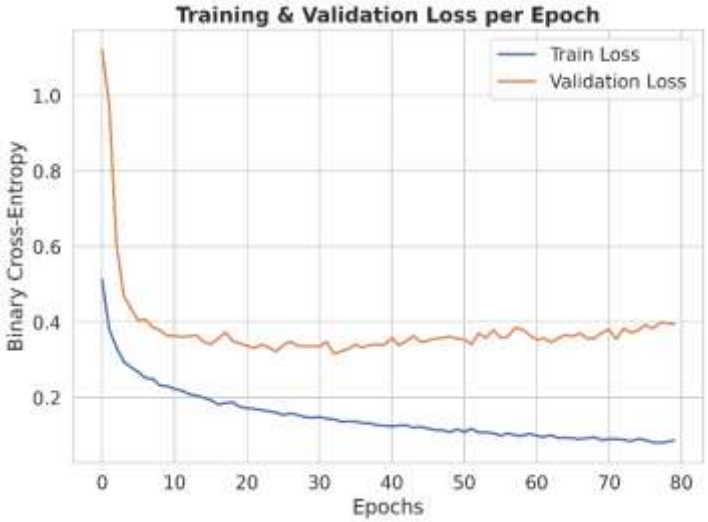

Figure 16 training loss for each epoch

7 Discussion

The experimental findings demonstrate that the Pocaii–DNN framework significantly outperforms conventional learning approaches for THz antenna classification. The model

10.48047/jocaaa.2024.33.07.63

benefits from two core advantages: (i) Adaptive hyperparameter evolution via Pocaii, which performs informed sampling across the hyperparameter space to avoid local minima, and (ii) Feature-driven representation learning through the DNN, enabling the discovery of non-linear relationships between geometrical and material parameters. Compared to the baseline DNN and GA-optimized variants, Pocaii–DNN achieved higher recall and F1-score, which is critical for classification systems where false negative minimization is essential. The confusion matrix indicated model stability, with only 51 false negatives despite significant dataset complexity. The ROC curve validated strong separability between GOOD and POOR antenna configurations. The correlation analysis revealed that antenna performance is influenced by a combination of structural and dielectric features. The weak correlation values suggest that learning must capture complex interactions rather than relying on single dominant predictors—a challenge effectively addressed by the proposed deep learning architecture. Moreover, convergence plots showed rapid stabilization during training, affirming the efficiency of the Pocaii-guided learning process. Unlike grid or random search optimization strategies, Pocaii contributes adaptability by maintaining balance between exploration and exploitation. This prevents premature convergence, a known limitation in GA-based tuning. The model's ability to generalize strongly across unseen antenna configurations demonstrates its suitability for electromagnetic engineering applications and AI-assisted antenna synthesis workflows.

8 Conclusion

The proposed Pocaii–DNN framework demonstrated a significant advancement in intelligent Terahertz (THz) antenna classification by integrating population-centric adaptive intelligence with deep neural learning. Unlike conventional hyperparameter tuning techniques, the Pocaii optimizer effectively explored complex search spaces and dynamically adapted learning configurations, while the DNN component provided a strong nonlinear feature representation capability. Experimental results confirmed the superiority of the proposed model, achieving an accuracy of 0.9250, precision of 0.9741, recall of 0.9466, and an F1-score of 0.9602, outperforming baseline DNN, POS-enhanced, and GA-optimized models. The high area under the ROC curve (0.923) further validated its discriminative strength, and the confusion matrix analysis revealed stability in predictions with minimal misclassification. Feature correlation analysis confirmed that the model captured complex geometric–electromagnetic relationships effectively without overfitting, supported by controlled convergence during training. Overall, the Pocaii–DNN model provides a reliable and scalable solution for AI-driven antenna

10.48047/jocaaa.2024.33.07.63

assessment and can be extended to electromagnetics-based design automation frameworks. Future research may focus on enhancing the model for multiclass antenna topology classification, integrating physics-informed learning constraints, and enabling end-to-end automated antenna synthesis through generative neural architectures.

9 Reference:

Chen, Y., Yan, L., & Han, C. (2021). Hybrid Spherical- and Planar-Wave Modeling and DCNN-Powered Estimation of Terahertz Ultra-Massive MIMO Channels. *IEEE Transactions on Communications*, *69*(10), 7063–7076. https://doi.org/10.1109/TCOMM.2021.3098696

Elburki, N., & Affes, S. (2024). A Machine Learning Approach for the Prediction of Indoor Propagation Path-Loss in the Tera-Hertz Bands. *IEEE Access*, *12*, 147527–147536. https://doi.org/10.1109/ACCESS.2024.3472549

Gezimati, M., & Singh, G. (2024). Terahertz Data Extraction and Analysis Based on Deep Learning Techniques for Emerging Applications. *IEEE Access*, *12*, 21174–21198. https://doi.org/10.1109/ACCESS.2024.3360930

Haque, M. A., Nahin, K. H., Nirob, J. H., Ahmed, M. K., Sawaran Singh, N. S., Paul, L. C., Algarni, A. D., ElAffendi, M., El-Latif, A. A. A., & Ateya, A. A. (2025). Multiband THz MIMO antenna with regression machine learning techniques for isolation prediction in IoT applications. *Scientific Reports*, *15*(1), 7701.

Haque, M. A., Nahin, K. H., Nirob, J. H., Ananta, R. A., Sawaran Singh, N. S., Paul, L. C., Algarni, A. D., ElAffendi, M., & Ateya, A. A. (2024). Machine learning-based novel-shaped THz MIMO antenna with a slotted ground plane for future 6G applications. *Scientific Reports*, *14*(1), 32162. https://doi.org/10.1038/s41598-024-79332-z

Karahan, E. A., Liu, Z., Gupta, A., Shao, Z., Zhou, J., Khankhoje, U., & Sengupta, K. (2024). Deep-learning enabled generalized inverse design of multi-port radio-frequency and sub-terahertz passives and integrated circuits. *Nature Communications*, *15*(1), 10734. https://doi.org/10.1038/s41467-024-54178-1

Li, J., Lei, H., Alavi, A. H., & Wang, G.-G. (2020). Elephant herding optimization: variants, hybrids, and applications. *Mathematics*, *8*(9), 1415.

Lin, A., Sun, W., Yu, H., Wu, G., & Tang, H. (2019). Adaptive comprehensive learning particle

10.48047/jocaaa.2024.33.07.63

swarm optimization with cooperative archive. *Applied Soft Computing*, *77*, 533–546.

Liu, H., Zhang, X., Liang, H., & Tu, L. (2020). Stability analysis of the human behavior-based particle swarm optimization without stagnation assumption. *Expert Systems with Applications*, *159*, 113638.

Ma, Z., Wu, G., Suganthan, P. N., Song, A., & Luo, Q. (2023). Performance assessment and exhaustive listing of 500+ nature-inspired metaheuristic algorithms. *Swarm and Evolutionary Computation*, *77*, 101248.

Mohammad Mubeena, & Dr. G. Udaykiran Bhargava. (n.d.). Predictive Modeling of Microstrip Antenna Parameters Through Feature-Enhanced Neural Network. *American Journal of Management and IOT Medical Computing*, *4*(3 SE-Articles), 52–64. https://doi.org/10.64751/ajmimc.2025.v4.n3.pp52-64

Peng, F., & Chen, X. (2024). An Antenna Optimization Framework Based on Deep Reinforcement Learning. *IEEE Transactions on Antennas and Propagation*, *PP*, 1. https://doi.org/10.1109/TAP.2024.3443411

Yadav, R., Gotra, S., Pandey, V. S., Sharma, A. K., & Verma, P. (2025). An Analytical and Mode Mapping Approach Using Machine Learning for Optimizing Hybrid Material-Based THz Antenna With Surface Plasmon Polaritons. *IEEE Transactions on Plasma Science*, *53*(3), 449–462. https://doi.org/10.1109/TPS.2025.3534289

Zhang, J.-Y., Yang, X., Ren, J.-J., Li, L.-J., Zhang, D.-D., Gu, J., & Xiong, W. (2024). Terahertz recognition of composite material interfaces based on ResNet-BiLSTM. *Measurement*, *233*, 114771. https://doi.org/https://doi.org/10.1016/j.measurement.2024.114771

Zhu, P., Wei, Z., Sfarra, S., Usamentiaga, R., Steenackers, G., Mandelis, A., Maldague, X., & Zhang, H. (2025). THz-Super-Resolution Generative Adversarial Network: Deep-Learning-Based Super-Resolution Imaging Using Terahertz Time-Domain Spectroscopy. *IEEE Transactions on Industrial Informatics*, *21*(9), 6660–6669. https://doi.org/10.1109/TII.2025.3567262